# Parametric Optimization and Comparative Photocatalytic Degradation of Acid Yellow 17 and Rhodamine B using $Na_{0.5}Bi_{0.5}FeO_3$ Nanoparticles

**Sanket Kumar[1], M. Meena[2], B.S. Meena[2], A.S. Shekhawat[3], U. Chandrawat[2*]**

**[1]Research Scholar, Department of Chemistry, Govt. College, Kota, Rajasthan, India**

**[2]Department of Chemistry, Govt. College, Kota, Rajasthan, India**

**[3]Department of Computer Science and Engineering, Manipal University Jaipur, Jaipur, Rajasthan, India**

*** Corresponding author**

**DOI: https://doi.org/10.51584/IJRIAS.2026.11110066**

**Received: 04 November 2026; Accepted: 11 November 2026; Published: 26 November 2026**

## ABSTRACT

The present study investigates the comparative photocatalytic degradation of Acid Yellow 17 (AY17), an anionic dye, and Rhodamine B (RhB), a cationic dye, using $Na_{0.5}Bi_{0.5}FeO_3$ nanoparticles calcined at 600, 700, and 800 °C under visible-light irradiation. The effects of irradiation time, initial dye concentration, catalyst dose, solution pH, and reaction temperature were evaluated, and the degradation kinetics were analyzed using the pseudo-first-order model. Both dyes showed improved degradation with increasing irradiation time and calcination temperature. After 80 min, the 800 °C catalyst achieved degradation efficiencies of 79% for AY17 and 87% for RhB, with apparent rate constants of 0.0181 and 0.0218 $min^{-1}$, respectively. An initial dye concentration of 40 mg $L^{-1}$ and a catalyst dose of 0.75 g $L^{-1}$ were identified as optimum under the investigated conditions. The optimum pH differed between the dyes, with maximum degradation observed at pH 6 for AY17 and pH 9 for RhB, highlighting the role of dye characteristics and catalyst surface charge in the degradation process. Increase in the reaction temperature from 25 to 35 °C further enhanced the degradation of both dyes. The experimental data showed good agreement with the pseudo-first-order kinetic model. Proposed degradation mechanisms involve photogenerated electron-hole pairs and reactive oxygen species (ROS), including hydroxyl and superoxide radicals, which contribute to dye transformation and possible mineralization. Hence, $Na_{0.5}Bi_{0.5}FeO_3$ nanoparticles calcined at 800 °C exhibited the highest photocatalytic performance, and RhB was degraded more efficiently than AY17 under the identical investigated conditions.

**Keywords:** $Na_{0.5}Bi_{0.5}FeO_3$ nanoparticles, photocatalysis, Acid Yellow 17, Rhodamine B, pseudo-first-order kinetics, calcination temperature, reactive oxygen species.

## INTRODUCTION

The textile industry holds a significant position in our country being the second-largest source of employment after agriculture and contributes greatly to the overall growth and development of the Indian economy. However, alongside this rapid growth and economic benefit, the industry has also contributed to environmental degradation due to the discharge of untreated liquid effluents into public sewage systems, surface water bodies such as rivers, ponds, and lakes, as well as agricultural land. The effluents generated from textile processes are typically hot, alkaline in nature, have a strong odor, and contain intense coloration due to the chemicals used during dyeing [1-2].

Dyes used in textile applications are generally classified based on their origin and the type of fibre to which they are applied. [3].

Azo dyes are extensively used not only in textiles but also in pharmaceuticals, cosmetics, food, paper, leather, and paint industries [4]. Acid Yellow 17 (AY17) is a mono- azo dye extensively employed for coloring various materials, including cotton, wool, silk, leather, paper, and hot-stamping foils [5,6]. In addition, AY17 finds applications in the printing and cosmetic industries [7-8].

Another dye, Rhodamine B (RhB), a xanthene dye, is widely used in the textile industry as a coloring agent because of its high stability and resistance to degradation [9-12]. It is also used as a biological stain and in various applications involving paper, drawing, food, leather, pharmaceutical products, cosmetics, and laboratory work. However, because of its toxic and carcinogenic properties, its use in food and cosmetic products has been restricted [13],[14]. The discharge of RhB into the environment can have harmful effects on

terrestrial and aquatic ecosystems [15], highlighting the need for effective methods of dye removal. Therefore, in view of this, the present study provides a comprehensive comparative study on how different operational parameters uniquely affect anionic vs. cationic dye degradation.

## Experimental Procedure

### Materials & Reagents

Acid Yellow 17 (AY17) and Rhodamine B (RhB) dyes were procured from SDS Fine Chem. (P) Ltd., India. HCl and NaOH were used to regulate the pH of the solutions. The molecular structures of AY17 and RhB dyes are presented in Figure 1. The AY17 and RhB dye exhibited a maximum absorption wavelength ($\lambda_{max}$) at 402 nm [16-18] and 554 nm [19,20] respectively, which was selected as the characteristic wavelength for monitoring its concentration during the photocatalytic degradation experiments.

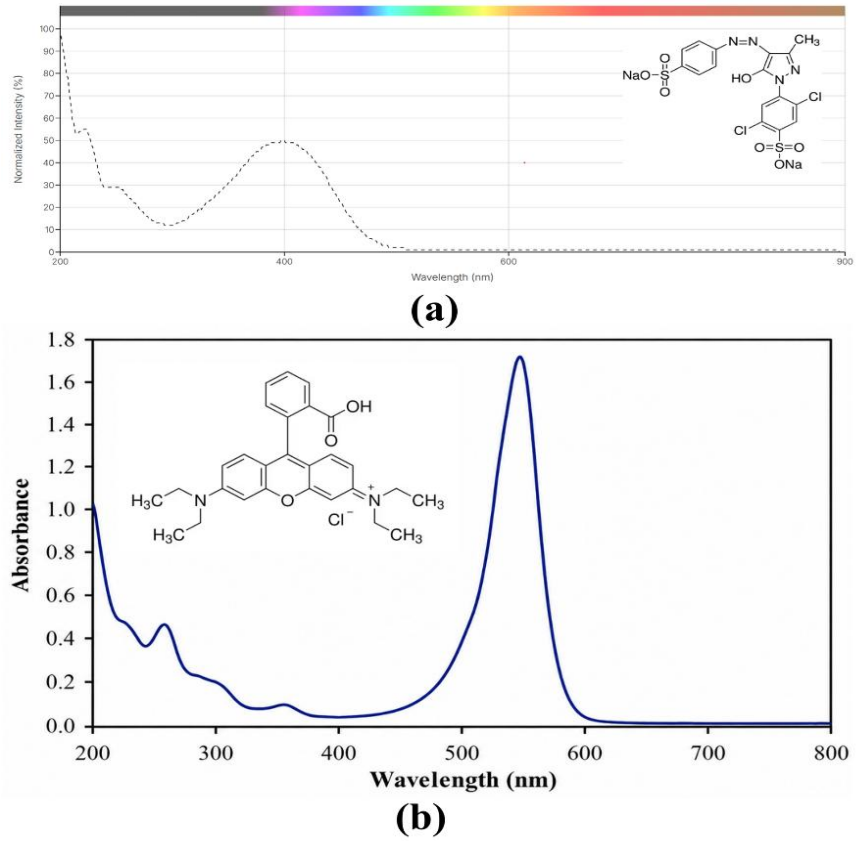


**Figure 1: Chemical structure of (a) AY17 dye ($\lambda_{max}$ = 402 nm) and (b) Rhodamine B dye ($\lambda_{max}$=554 nm)**

### Photocatalytic Experimental Setup:

Photocatalytic activity was investigated using a cylindrical glass reactor equipped with a centrally positioned glass tube housing a 500 W Xe arc lamp with an irradiation intensity of 137 mW $cm^{-2}$, which served as the

light source for illuminating the dye solution. A magnetic stirrer placed at the base of the reactor ensured continuous mixing and uniform dispersion of the photocatalyst throughout the reaction medium. Before light exposure, the reaction mixture was kept under dark conditions for 15 minutes to allow the dye molecules to interact and equilibrate with the photocatalyst surface. After initiating visible light irradiation, aliquots were periodically collected from the reaction mixture at fixed time intervals and analysed for residual dye quantity using a UV–Vis spectrophotometer at a λ of 402nm (AY17 dye) and 554nm (RhB dye). The photocatalytic activity of the catalyst was subsequently evaluated using the following Eq. (1):

$$\text{Degradation } \% = \frac{C_o - C_t}{C_o} \times 100 \qquad (1)$$

Here, $C_0$ (mg/L) denotes the dye concentration in the solution following dark adsorption equilibrium, whereas $C_t$ (mg/L) represents the dye concentration at irradiation time t. A series of controlled experiments was performed to evaluate how irradiation duration influences dye removal through the photocatalytic process.

The photocatalytic degradation of AY 17 and RhB by the catalyst was systematically optimized across different operational parameters. The catalyst calcined at all three temperatures (600 °C, 700 °C, 800 °C) gave the best degradation results at 40 ppm dye concentration, 0.75 g $L^{-1}$ catalyst dose, and a reaction temperature of 35 °C. However, the system exhibited distinct pH selectivity, achieving maximum degradation at pH 6 for AY and pH 9 for RhB. These optimized parameters maximize reactive oxygen species (ROS) generation and kinetic collisions while mitigating nanoparticle agglomeration and light-screening effects. Furthermore, the distinct pH optima arise from highly favorable electrostatic attractions between the specific ionic dyes and the catalyst's pH-dependent surface charge.

## RESULTS AND DISCUSSION

### Preparation of catalyst

Stoichiometric metal nitrates were dissolved in water, and a citric acid-assisted Pechini sol-gel technique was used to prepare $Na_{0.5}Bi_{0.5}FeO_3$ nanopowders. To create a homogeneous gel, the metal ions were chelated with citric acid and polymerized using ethylene glycol at 90 °C (pH ~8.0). To produce the final nanoparticles, the dried gel was first pre-calcined and then calcined for four hours at 600–800 °C. A highly crystalline, phase-pure orthorhombic $Na_{0.5}Bi_{0.5}FeO_3$ structure was confirmed by XRD analysis, with excellent structural ordering and sharp diffraction peaks attained at a calcination temperature of 600 °C. FTIR spectra, which showed distinctive Fe-O-Fe and O-Fe-O vibrational bands at 545 $cm^{-1}$ and 605 $cm^{-1}$, further confirmed the perovskite metal-oxygen framework. Furthermore, UV-Vis spectroscopy demonstrated a wide-band-gap semiconducting nature, with the optical band gap progressively narrowing from 2.10 eV to 1.85 eV as the calcination temperature increased to 800 °C.

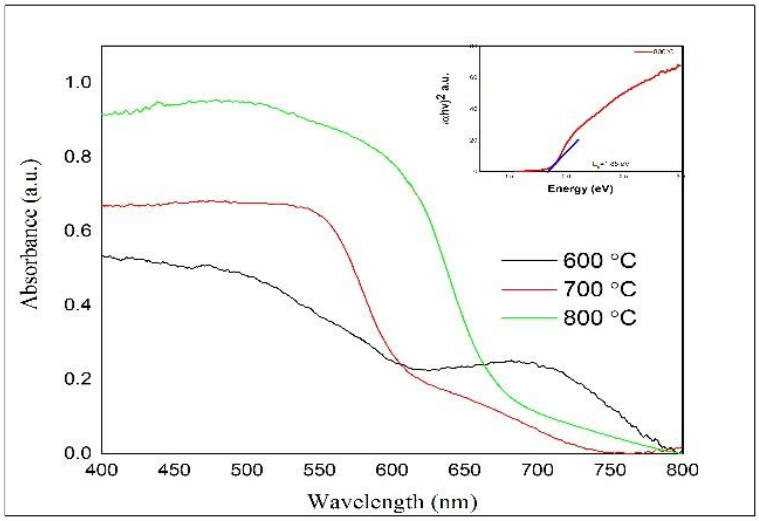


**Figure 2: UV-Vis. spectra of $Na_{0.5}Bi_{0.5}FeO_3$ obtained after calcination at temperatures 600 °C, 700 °C and 800 °C. Tauc plot for determining the direct band gap (inset).**

ISSN No. 2454-6194 | DOI: 10.51584/IJRIAS |Volume XI Issue XI November 2026

**Effect of Irradiation Time:**

The photocatalytic degradation of both Acid Yellow 17 (AY17) and Rhodamine B (RhB) increased progressively with irradiation time, with the highest degradation achieved using $Na_{0.5}Bi_{0.5}FeO_3$ nanoparticles calcined at 800 °C, followed by those calcined at 700 °C and 600 °C. After 80 min, AY17 degradation reached 79%, 73%, and 67%, respectively, whereas RhB degradation reached 87.0%, 81.5%, and 71.5% under the same calcination conditions. These results indicate that RhB degraded more efficiently than AY17 for all three catalysts.

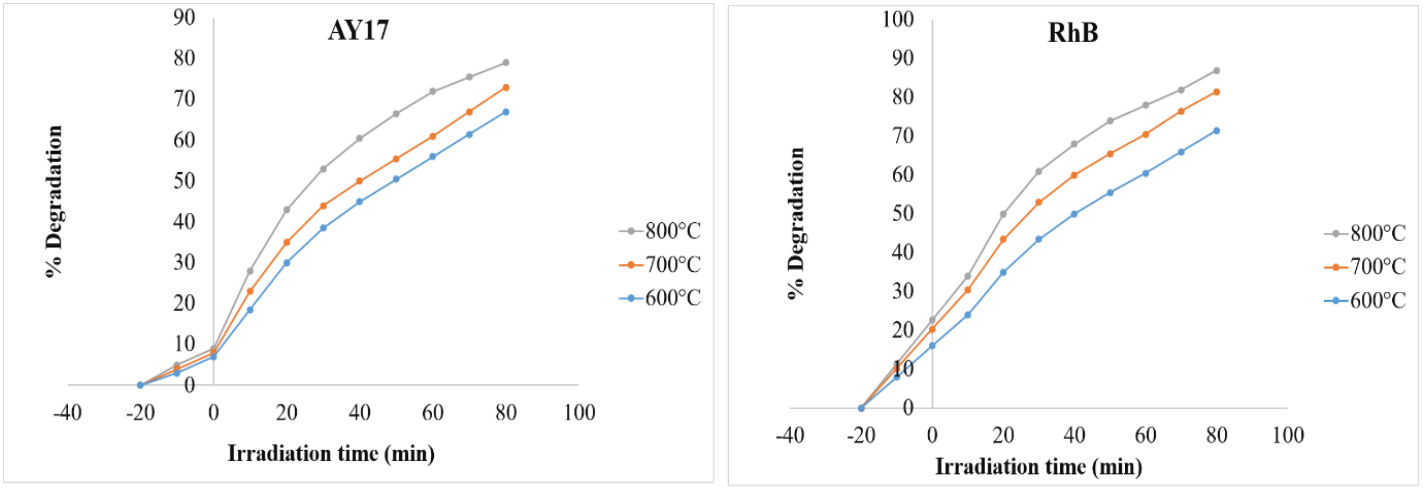


**Figure 3: Effect of irradiation time on the photocatalytic degradation of AY17 and RhB using $Na_{0.5}Bi_{0.5}FeO_3$ nanoparticles calcined at different temperatures. (Experimental conditions: [dye] = 40 ppm; Catalyst Dose= 0.75 g $L^{-1}$; pH = 6.0 (AY 17); pH = 9.0 (RhB); temperature = 308 K]**

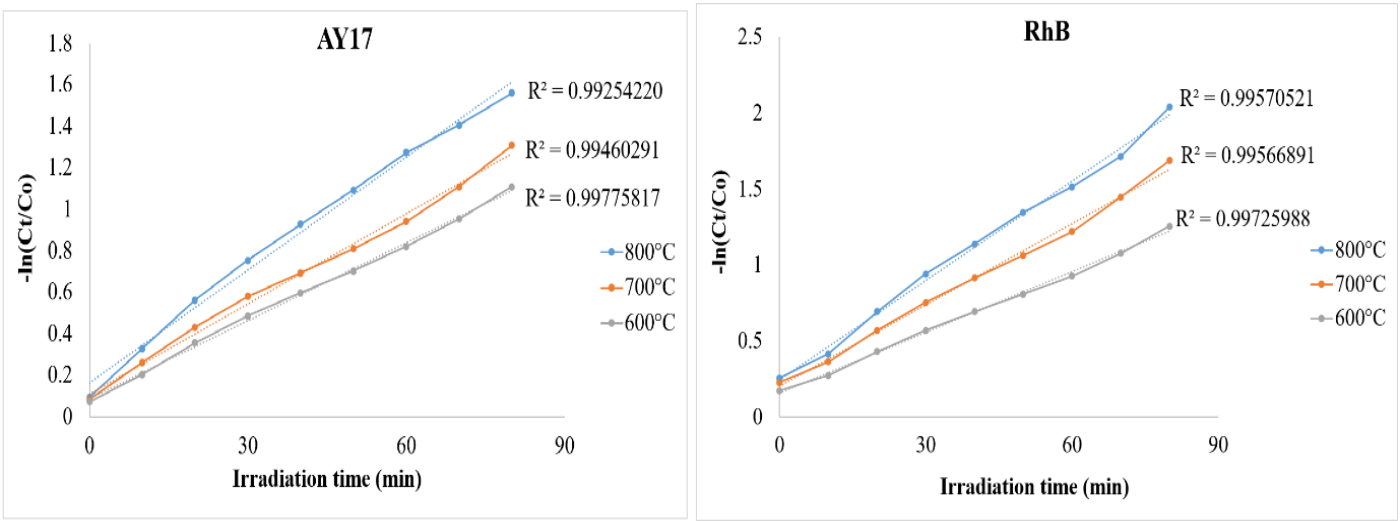


**Figure 4: Pseudo-first-order kinetic plots for the degradation of AY17 and RhB using $Na_{0.5}Bi_{0.5}FeO_3$ nanoparticles calcined at different temperatures. (Experimental conditions: [dye] = 40 ppm; Catalyst Dose= 0.75 g $L^{-1}$; pH = 6.0 (AY 17); pH = 9.0 (RhB); temperature = 308 K]**

The reaction kinetics of the photocatalytic degradation were evaluated using the Langmuir-Hinshelwood (L-H) model, and Kapp is determined from the slope of -ln Ct/Co vs. time.

The kinetic results supported this trend, with the apparent rate constant (Kapp) for AY17 increasing from 0.01257 to 0.0181 $min^{-1}$, while that for RhB increased from 0.01329 to 0.02180 $min^{-1}$ as the calcination temperature of the photocatalyst increased from 600 to 800 °C. The high $R^2$ values for both dyes (0.9925–0.9978 for AY17 and 0.9956–0.9972 for RhB) indicated good agreement with the pseudo-first-order kinetic model. The improved photocatalytic activity at higher calcination temperatures may be associated with enhanced crystallinity and more effective visible-light utilization. The suitability of Bismuth based materials

ISSN No. 2454-6194 | DOI: 10.51584/IJRIAS |Volume XI Issue XI November 2026

for visible-light photocatalysis has been reported previously, with dye degradation attributed to the generation and separation of photogenerated charge carriers [21,22]. Efficient charge separation can reduce electron–hole recombination and promote the formation of reactive species involved in dye oxidation [23-25].

**Table 1: Pseudo-first-order kinetic parameters for the degradation of AY17 and RhB using $Na_{0.5}Bi_{0.5}FeO_3$ nanoparticles calcined at different temperatures. (Experimental conditions: [Initial dye] = 40 ppm; Catalyst Dose= 0.75 g $L^{-1}$; pH = 6.0 (AY 17); pH = 9.0 (RhB); Temperature = 308 K]**

| S. No. | Sample | AY17 | | RhB | |
|---|---|---|---|---|---|
| | | Kapp ($min^{-1}$) | $R^2$ | Kapp ($min^{-1}$) | $R^2$ |
| 1 | 600°C | 0.01257 | 0.99776 | 0.01329 | 0.9972 |
| 2 | 700°C | 0.0145 | 0.9946 | 0.01784 | 0.9956 |
| 3 | 800°C | 0.0181 | 0.99254 | 0.0218 | 0.99571 |

**Effect of Initial Dye Concentration:**

The photocatalytic degradation of both Acid Yellow 17 (AY17) and Rhodamine B (RhB) increased with initial dye conc. from 20 to 40 mg $L^{-1}$, followed by a decline at 50 mg $L^{-1}$ for all three $Na_{0.5}Bi_{0.5}FeO_3$ catalysts. At the optimum concentration of 40 mg $L^{-1}$, AY17 degradation reached 67%, 73%, and 79% using catalysts calcined at 600, 700, and 800 °C, respectively, while RhB degradation reached 78.13%, 81.50%, and 87.0% under similar conditions.

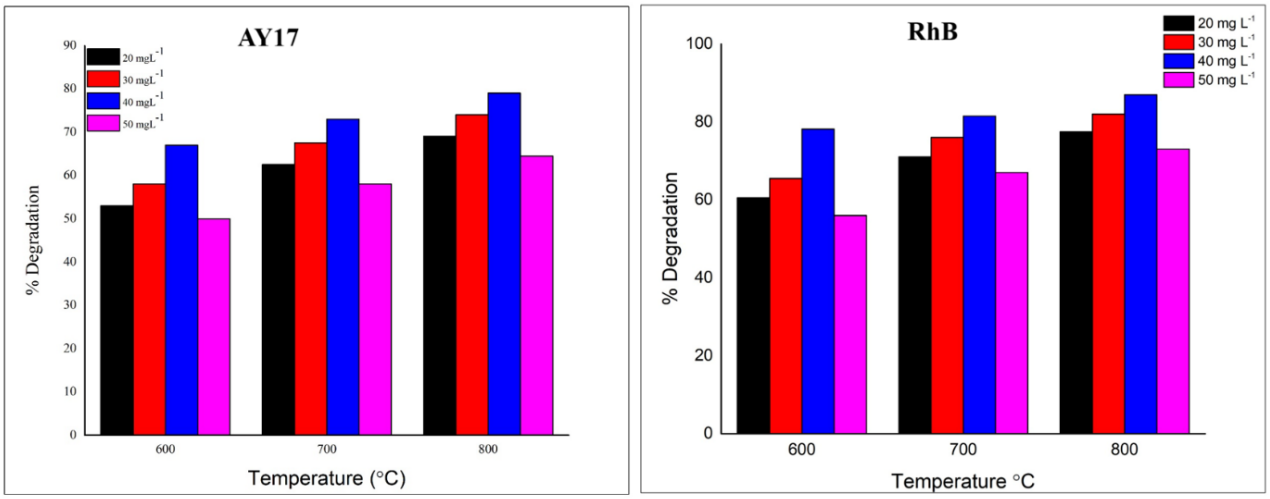


**Figure 5: Effect of initial AY17 and RhB concentration on the photocatalytic degradation using $Na_{0.5}Bi_{0.5}FeO_3$ nanoparticles calcined at 600 °C, 700 °C and 800 °C. (Experimental conditions: [Initial dye] = 20, 30, 40 and 50 ppm; Catalyst Dose= 0.75 g $L^{-1}$; pH = 6.0 (AY 17); pH = 9.0 (RhB); Temperature = 308 K]**

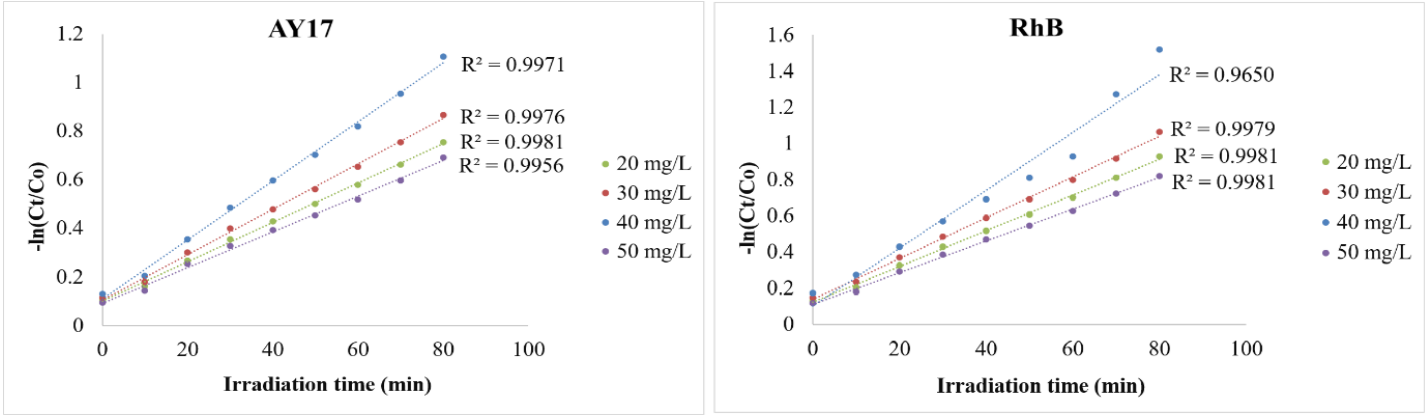


**(a)**

ISSN No. 2454-6194 | DOI: 10.51584/IJRIAS |Volume XI Issue XI November 2026

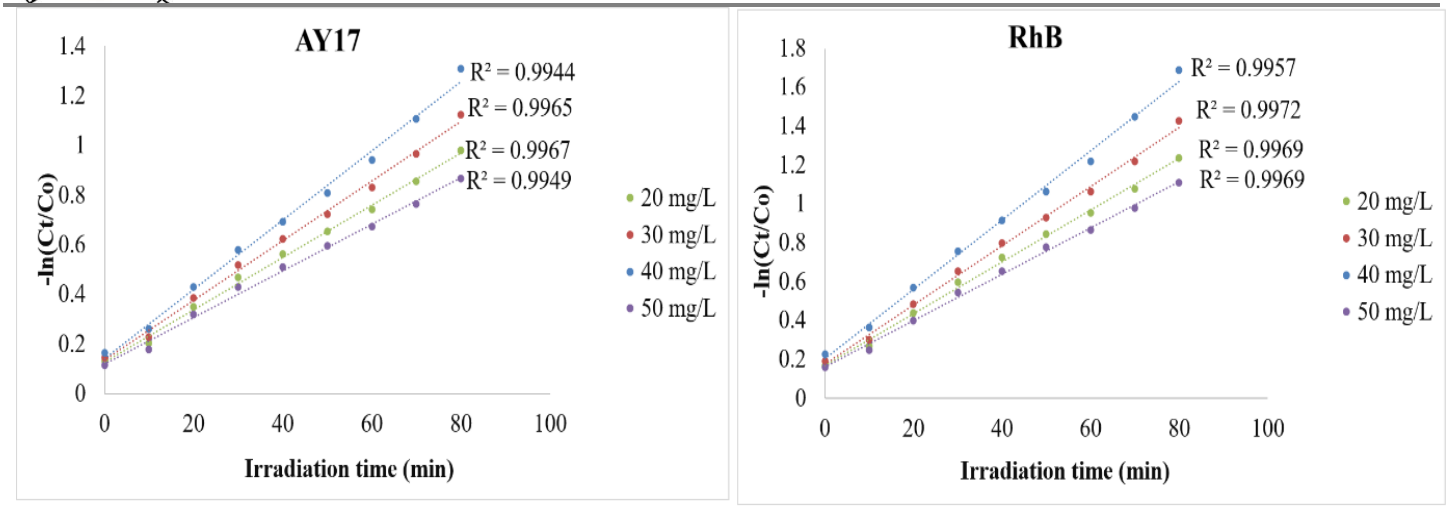


(b)

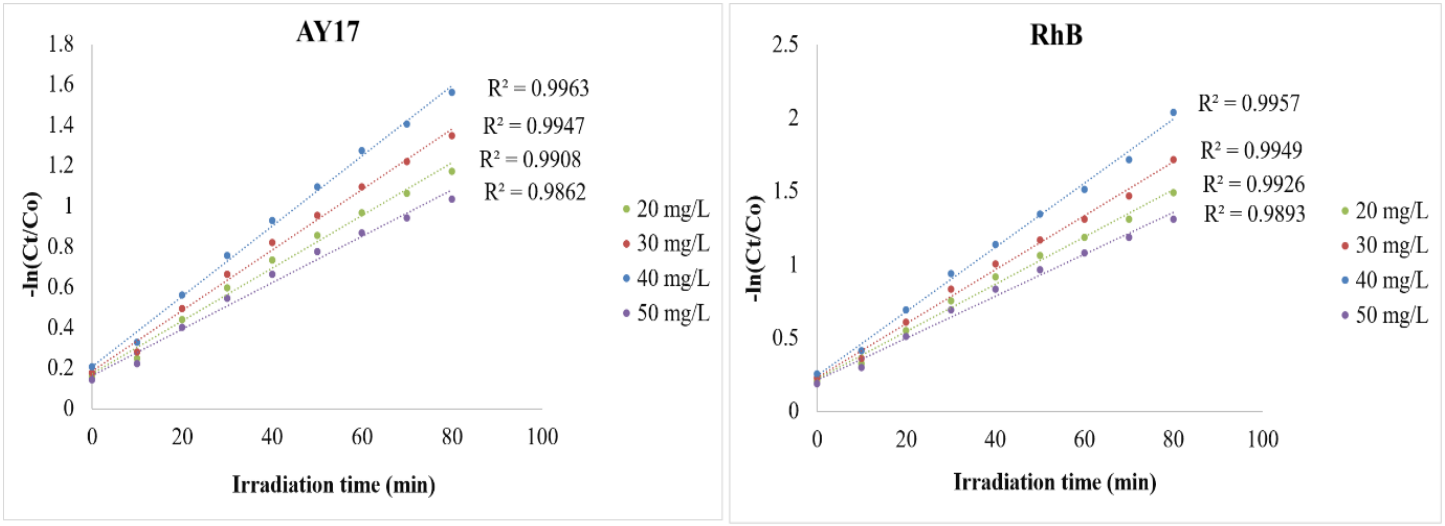


(c)

**Figure 6: Pseudo-first-order kinetic plots for the degradation of AY17 and RhB at varying initial dye concentrations using $Na_{0.5}Bi_{0.5}FeO_3$ nanoparticles calcined at (a) 600 °C (b) 700 °C (c) 800 °C. (Experimental conditions: [Initial dye] = 20, 30, 40 and 50 ppm; Catalyst Dose= 0.75 g $L^{-1}$; pH = 6.0 (AY 17); pH = 9.0 (RhB); Temperature = 308 K]**

The apparent rate constants (Kapp) for AY17 were 0.0122, 0.0139, and 0.0174 $min^{-1}$, whereas those for RhB were 0.0160, 0.0178, and 0.0218 $min^{-1}$, respectively. These results indicate that RhB exhibited higher degradation efficiency and faster photocatalytic degradation than AY17 at each calcination temperature. The decrease in degradation efficiency and rate constant at 50 mg $L^{-1}$ may be attributed to increased dye adsorption on the catalyst surface and greater absorption and scattering of incident light, which reduce light penetration and the availability of photons for photocatalytic reactions. Similar concentration-dependent behavior has been reported for AY17 and RhB degradation using Ag@$TiO_2$ and other photocatalysts [26-29].

In both cases, the catalyst calcined at 800 °C exhibited the highest photocatalytic activity, suggesting that calcination temperature played an important role in determining degradation performance. The improved activity may be associated with favourable structural and optical properties, as higher crystallinity and smaller crystallite size have been linked to enhanced RhB degradation by bismuth-based nanoparticles [30].

Furthermore, calcination temperature can influence the phase composition, crystallite size, and energy-gap properties of ferrite photocatalysts [31], while improved visible-light photocatalytic performance has also been reported for other Ni and Zn-based doped materials [32–35]. Thus, 40 mg $L^{-1}$ was identified as the optimum

ISSN No. 2454-6194 | DOI: 10.51584/IJRIAS |Volume XI Issue XI November 2026

initial concentration for both dyes, and RhB showed better photocatalytic degradation than AY17 under the investigated conditions.

**Table 2: Pseudo-first-order kinetic parameters for the degradation of AY17 and RhB at different initial dye concentrations using $Na_{0.5}Bi_{0.5}FeO_3$ nanoparticles calcined at (A) 600 °C (B) 700 °C (C) 800 °C. (Experimental conditions: [Initial dye] = 20, 30, 40 and 50 ppm; Catalyst Dose= 0.75 g $L^{-1}$; pH = 6.0 (AY 17); pH = 9.0 (RhB); Temperature = 308 K]**

| S. No. | $C_0$ (mg $L^{-1}$) | AY17 | | | RhB | | |
|---|---|---|---|---|---|---|---|
| | | Kapp ($min^{-1}$) | Rate (mg $L^{-1}$ $min^{-1}$) | $R^2$ | Kapp ($min^{-1}$) | Rate (mg $L^{-1}$ $min^{-1}$) | $R^2$ |
| 1 | 20 | 0.0081 | 0.162 | 0.998 | 0.0099 | 0.198 | 0.9981 |
| 2 | 30 | 0.0093 | 0.279 | 0.998 | 0.0113 | 0.339 | 0.9979 |
| 3 | 40 | 0.0122 | 0.488 | 0.997 | 0.016 | 0.64 | 0.965 |
| 4 | 50 | 0.0073 | 0.365 | 0.996 | 0.0088 | 0.44 | 0.9981 |

**(a)**

| S. No. | $C_0$ (mg $L^{-1}$) | AY17 | | | RhB | | |
|---|---|---|---|---|---|---|---|
| | | Kapp ($min^{-1}$) | Rate (mg $L^{-1}$ $min^{-1}$) | $R^2$ | Kapp ($min^{-1}$) | Rate (mg $L^{-1}$ $min^{-1}$) | $R^2$ |
| 1 | 20 | 0.0105 | 0.21 | 0.9967 | 0.0133 | 0.266 | 0.9969 |
| 2 | 30 | 0.012 | 0.36 | 0.9965 | 0.0152 | 0.456 | 0.9972 |
| 3 | 40 | 0.0139 | 0.556 | 0.9944 | 0.0178 | 0.712 | 0.9957 |
| 4 | 50 | 0.0094 | 0.47 | 0.9967 | 0.0119 | 0.595 | 0.9969 |

**(b)**

| S. No. | $C_0$ (mg $L^{-1}$) | AY17 | | | RhB | | |
|---|---|---|---|---|---|---|---|
| | | Kapp ($min^{-1}$) | Rate (mg $L^{-1}$ $min^{-1}$) | $R^2$ | Kapp ($min^{-1}$) | Rate (mg $L^{-1}$ $min^{-1}$) | $R^2$ |
| 1 | 20 | 0.013 | 0.26 | 0.9908 | 0.0161 | 0.322 | 0.9926 |
| 2 | 30 | 0.015 | 0.45 | 0.9947 | 0.0184 | 0.552 | 0.9949 |
| 3 | 40 | 0.0174 | 0.696 | 0.9963 | 0.0218 | 0.872 | 0.9957 |
| 4 | 50 | 0.0115 | 0.575 | 0.9862 | 0.0142 | 0.71 | 0.9893 |

**(c)**

**Effect of Catalyst Dose**

For both Acid Yellow 17 (AY17) and Rhodamine B (RhB), photocatalytic degradation increased with increasing $Na_{0.5}Bi_{0.5}FeO_3$ catalyst dose from 0.25 to 0.75 g $L^{-1}$, followed by a slight decline at 1.0 g $L^{-1}$. At the optimum dose of 0.75 g $L^{-1}$, AY17 degradation reached 67.13%, 73.13%, and 79.13% for the catalysts calcined at 600, 700, and 800 °C, respectively, while RhB degradation reached 78.13%, 81.50%, and 87.0% under the same conditions.

ISSN No. 2454-6194 | DOI: 10.51584/IJRIAS |Volume XI Issue XI November 2026

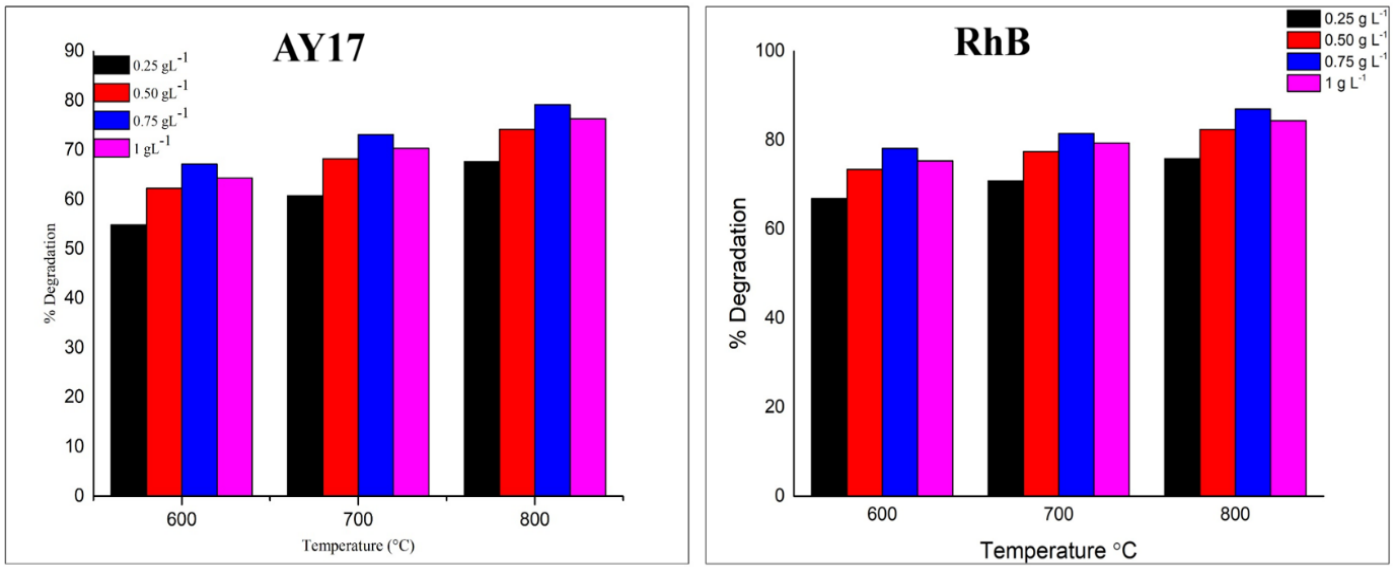


**Figure 7: Effect of $Na_{0.5}Bi_{0.5}FeO_3$ catalyst dose on the photocatalytic degradation of AY17 and RhB using nanoparticles calcined at 600 °C, 700 °C and 800 °C. (Experimental conditions: [dye] = 40 ppm; catalyst dose = 0.25, 0.50, 0.75 and 1.00 g $L^{-1}$; pH = 6.0 (AY 17); pH = 9.0 (RhB); temperature = 308 K]**

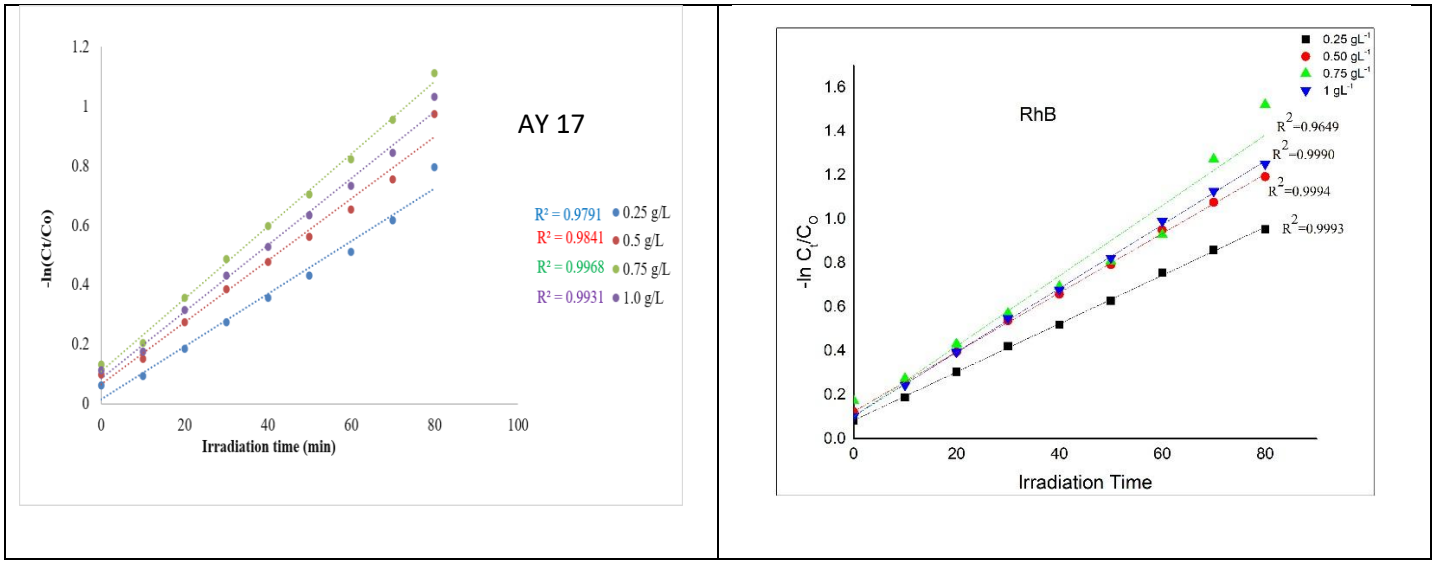


**(A)**

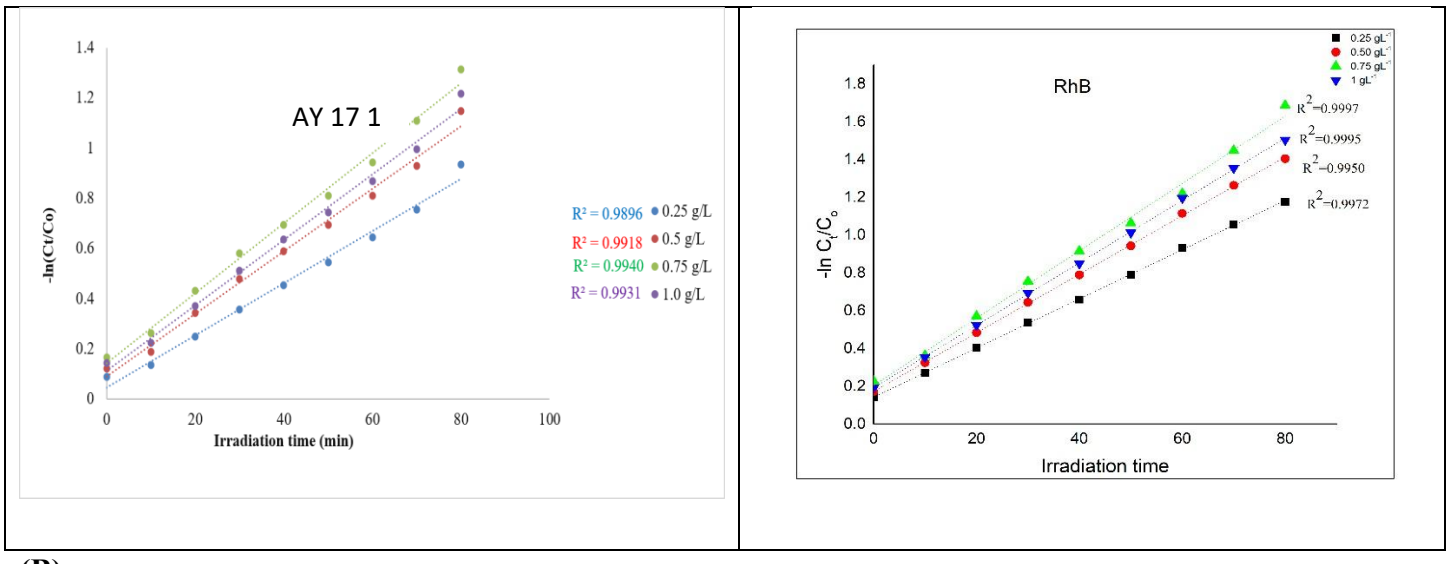


**(B)**

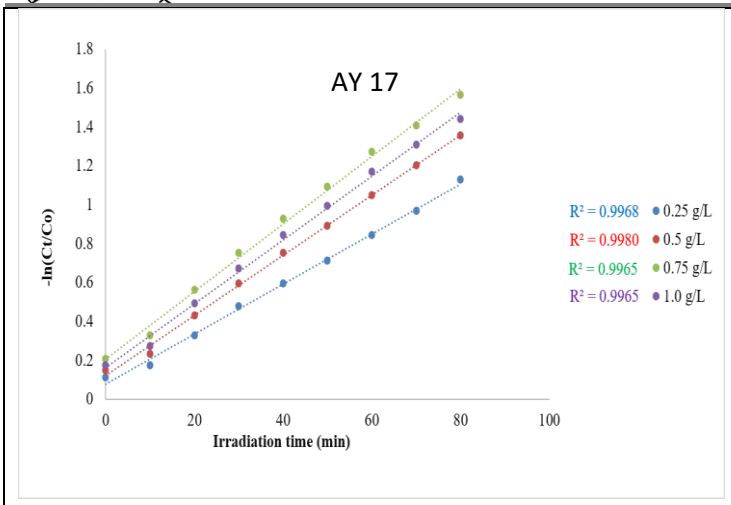


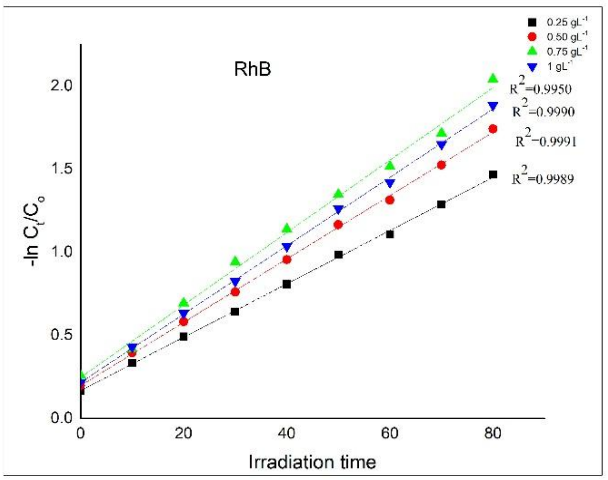


**(C)**

**Figure 8: Pseudo-first-order kinetic plots for the degradation of AY17 and RhB at different $Na_{0.5}Bi_{0.5}FeO_3$ catalysts calcined (a) 600 °C (b) 700 °C (c) 800 °C. (Experimental conditions: [dye] = 40 ppm; catalyst dose = 0.25, 0.50, 0.75 and 1.00 g $L^{-1}$; pH = 6.0 (AY 17); pH = 9.0 (RhB); temperature = 308 K]**

The apparent rate constants (Kapp) for AY17 were 0.0122, 0.0140, and 0.0174 $min^{-1}$ for the 600, 700, and 800 °C samples, respectively. These results demonstrate that RhB exhibited higher degradation efficiency than AY17 at each calcination temperature. The initial increase in degradation for both dyes can be attributed to the availability of more photocatalytic active sites and greater contact between dye molecules and the catalyst surface. However, excessive catalyst loading may cause particle agglomeration and increased light scattering or shielding, thereby reducing light penetration and limiting photocatalytic efficiency. Similar dependence of AY17 degradation on catalyst concentration has been reported for PANI–$TiO_2$ systems [36], while studies using Fe-based advanced oxidation processes have also highlighted the importance of catalyst concentration in controlling AY17 degradation [37]. For RhB, the influence of photocatalyst amount on degradation using bismuth-based nanoparticles has been investigated [29], and an optimum catalyst dosage has also been reported for ferrite-based catalysts [38]. The importance of surface properties in dye removal is further supported by the higher RhB adsorption observed for ferrite nanoparticles with greater surface area and porosity [39]. In addition, the higher photocatalytic activity of the 800 °C sample agrees with reports highlighting the influence of structural and charge-transfer characteristics on Zn-based nanoparticles' photocatalytic performance [31,32]. Thus, 0.75 g $L^{-1}$ was identified as the optimum catalyst dose for both dyes, and the catalyst calcined at 800 °C exhibited the highest degradation efficiency.

**Table 3: Pseudo-first-order kinetic parameters for the degradation of AY17 and RhB at different $Na_{0.5}Bi_{0.5}FeO_3$ catalyst doses calcined (a) 600 °C (b) 700 °C (c) 800 °C. (Experimental conditions: [dye] = 40 ppm; catalyst dose = 0.25, 0.50, 0.75 and 1.00 g $L^{-1}$; pH = 6.0 (AY 17); pH = 9.0 (RhB); temperature = 308 K]**

| S. No. | Catalyst Dose (g $L^{-1}$) | AY17 | | RhB | |
|---|---|---|---|---|---|
| | | Kapp ($min^{-1}$) | $R^2$ | Kapp ($min^{-1}$) | $R^2$ |
| 1 | 0.25 | 0.0088 | 0.9791 | 0.01101 | 0.9993 |
| 2 | 0.5 | 0.0104 | 0.9841 | 0.01352 | 0.9994 |
| 3 | 0.75 | 0.0122 | 0.9968 | 0.01602 | 0.9649 |
| 4 | 1 | 0.0112 | 0.9931 | 0.01452 | 0.999 |

**(a)**

ISSN No. 2454-6194 | DOI: 10.51584/IJRIAS |Volume XI Issue XI November 2026

| S. No. | Catalyst Dose (g $L^{-1}$) | AY17 | | RhB | |
|---|---|---|---|---|---|
| | | Kapp ($min^{-1}$) | $R^2$ | Kapp ($min^{-1}$) | $R^2$ |
| 1 | 0.25 | 0.0104 | 0.9896 | 0.01301 | 0.9972 |
| 2 | 0.5 | 0.0125 | 0.9918 | 0.01551 | 0.995 |
| 3 | 0.75 | 0.014 | 0.994 | 0.01784 | 0.9997 |
| 4 | 1 | 0.0131 | 0.9931 | 0.01652 | 0.9995 |

**(b)**

| S. No. | Catalyst Dose (g $L^{-1}$) | AY17 | | RhB | |
|---|---|---|---|---|---|
| | | Kapp ($min^{-1}$) | $R^2$ | Kapp ($min^{-1}$) | $R^2$ |
| 1 | 0.25 | 0.0129 | 0.9968 | 0.01605 | 0.9989 |
| 2 | 0.5 | 0.0154 | 0.998 | 0.01906 | 0.9991 |
| 3 | 0.75 | 0.0174 | 0.9965 | 0.0218 | 0.995 |
| 4 | 1 | 0.0164 | 0.9965 | 0.02051 | 0.999 |

**(c)**

**Effect of Initial pH**

The effect of pH on the photocatalytic degradation of Acid Yellow 17 (AY17) and Rhodamine B (RhB) showed distinct trends under the investigated conditions. For AY17, the efficiency increased with pH from 4 to 6 and then decreased at pH 7 and 8 for all three $Na_{0.5}Bi_{0.5}FeO_3$ samples. At pH 6, the degradation efficiencies reached approximately 67%, 73%, and 79% for the catalysts calcined at 600, 700, and 800 °C, respectively. The decline at higher pH suggests that changes in the surface charge of the catalyst and interactions between the catalyst surface and dye molecules may influence degradation. In contrast, RhB degradation increased from pH 6 to pH 9 and then decreased at pH 10. At pH 9, the degradation efficiencies were 71.5%, 81.5%, and 87.0% for the 600, 700, and 800 °C samples, respectively. The lower degradation at pH 10 indicates that strongly alkaline conditions were less favourable than pH 9 under the present experimental conditions.

Comparatively, the optimum pH differed between the two dyes, with AY17 showing maximum degradation at pH 6 and RhB at pH 9. This difference may be associated with the distinct chemical structures and ionic characteristics of the dyes, which affect their interactions with the catalyst surface and the availability of reactive species during photocatalysis. Despite the different pH optima, both dyes followed the same calcination-temperature trend, with the 800 °C sample exhibiting the highest degradation, followed by the 700 and 600 °C samples. The improved performance of the higher-temperature sample may be related to its structural and optical properties, which can influence photogenerated charge-carrier behaviour.

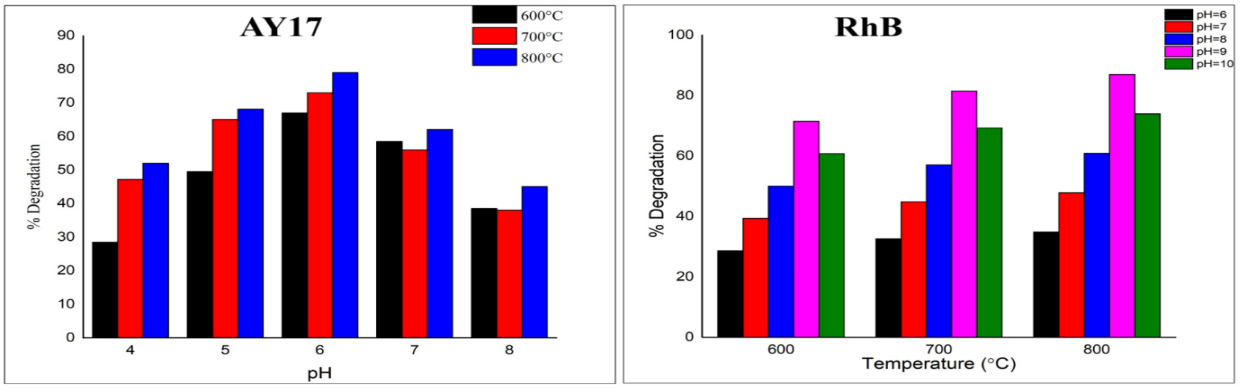


**Figure 9: Effect of varying pH on the degradation of AY17 and RhB using $Na_{0.5}Bi_{0.5}FeO_3$ nanoparticles**

ISSN No. 2454-6194 | DOI: 10.51584/IJRIAS |Volume XI Issue XI November 2026

**calcined at 600 °C, 700 °C and 800 °C. (Experimental conditions: [dye] = 40 mg $L^{-1}$; catalyst = 0.75 g $L^{-1}$; pH = 4–8 for AY17 and pH = 6–10 for RhB; temperature = 308 K]**

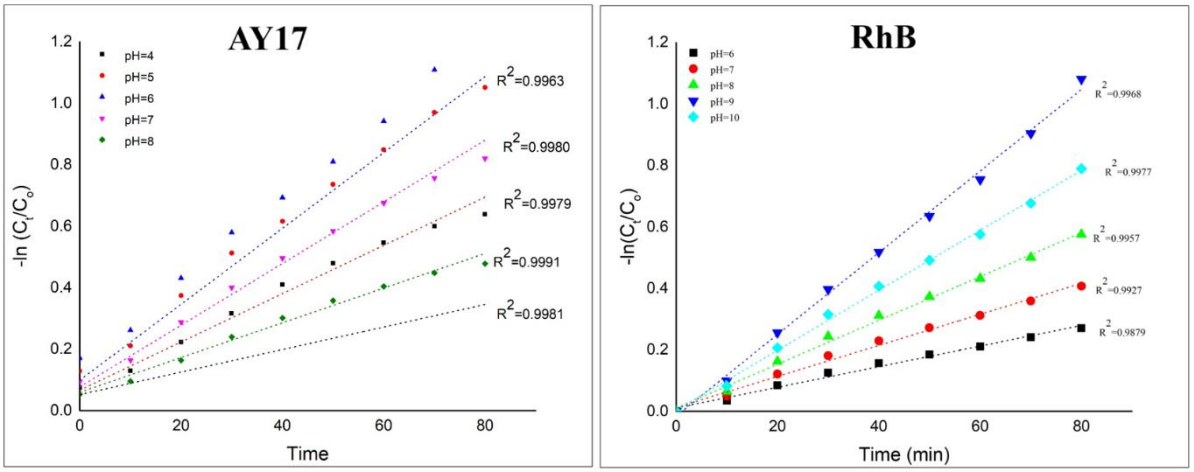


**(a)**

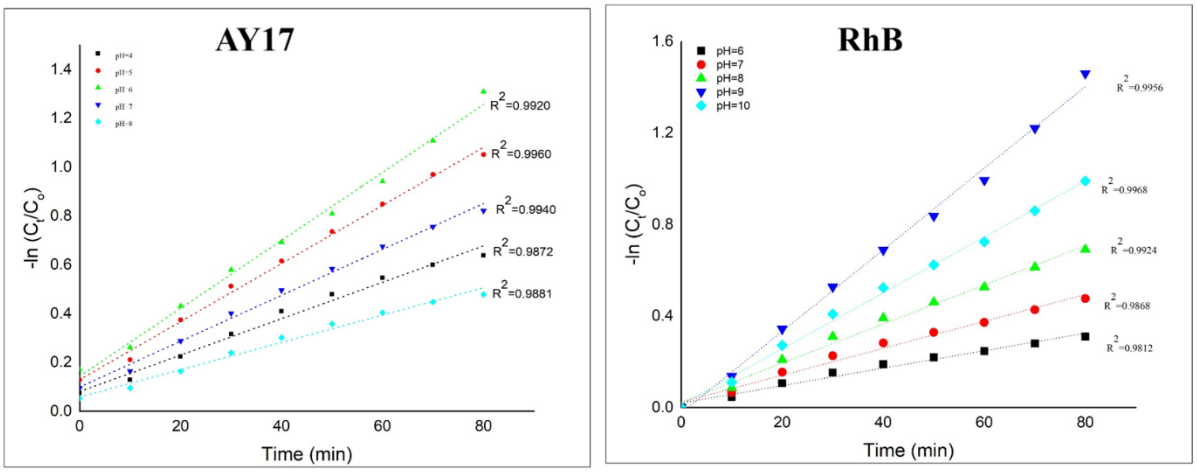


**(b)**

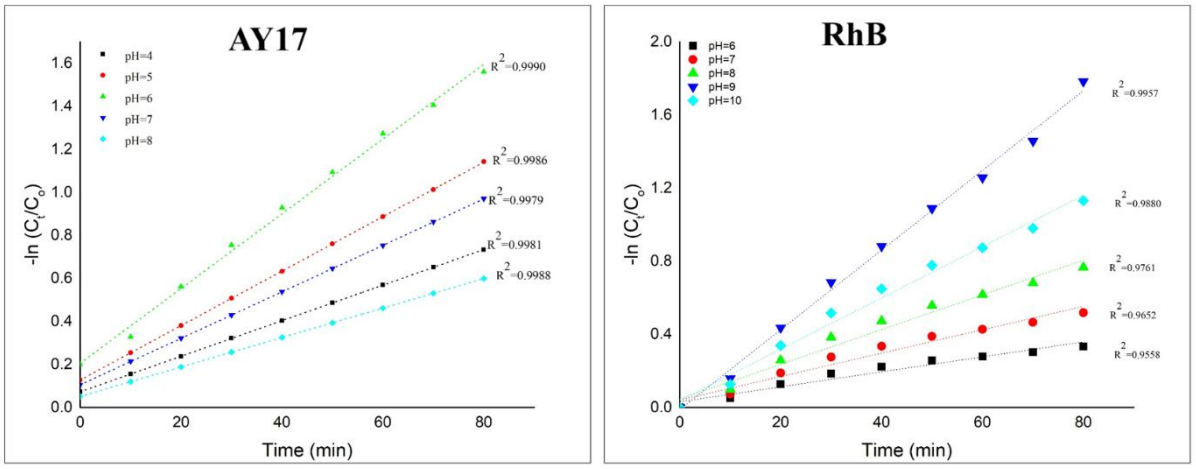


**(c)**

**Figure 10: Pseudo-first-order kinetic plots for the degradation of AY17 and RhB at different pH values using $Na_{0.5}Bi_{0.5}FeO_3$ nanoparticles calcined at (a) 600 °C, (b) 700 °C and (c) 800 °C. (Experimental conditions: [dye] = 40 mg $L^{-1}$; catalyst = 0.75 g $L^{-1}$; pH = 4–8 for AY17 and pH = 6–10 for RhB; temperature = 308 K]**

**Table 4: Comparison of pseudo-first-order Kapp for the photocatalytic degradation of AY17 and RhB at different pH values using $Na_{0.5}Bi_{0.5}FeO_3$ nanoparticles calcined at (a) 600 °C, (b) 700 °C and (c) 800 °C. (Experimental conditions: [dye] = 40 mg $L^{-1}$; catalyst = 0.75 g $L^{-1}$; pH = 4–8 for AY17 and pH = 6–10 for RhB; temperature = 308 K]**

| Catalyst | AY 17 | | RhB | |
|---|---|---|---|---|
| | pH | $K_{app}$ ($min^{-1}$) | pH | $K_{app}$ ($min^{-1}$) |
| | 4 | 0.0036 | 6 | 0.00335 |
| | 5 | 0.0078 | 7 | 0.00505 |
| $Na_{0.5}Bi_{0.5}FeO_3$, 600 °C | 6 | 0.0123 | 8 | 0.00713 |
| | 7 | 0.01 | 9 | 0.01329 |
| | 8 | 0.0055 | 10 | 0.00976 |
| | 4 | 0.00746 | 6 | 0.00382 |
| $Na_{0.5}Bi_{0.5}FeO_3$, 700 °C | 5 | 0.0119 | 7 | 0.00588 |
| | 6 | 0.01392 | 8 | 0.00855 |
| | 7 | 0.0094 | 9 | 0.1784 |
| | 8 | 0.00559 | 10 | 0.0122 |
| | 4 | 0.00827 | 6 | 0.0041 |
| $Na_{0.5}Bi_{0.5}FeO_3$, 800 °C | 5 | 0.01267 | 7 | 0.0064 |
| | 6 | 0.01738 | 8 | 0.0095 |
| | 7 | 0.01081 | 9 | 0.0218 |
| | 8 | 0.00685 | 10 | 0.014 |

**Effect of Reaction Temperature & Thermodynamics**

The degradation of both Acid Yellow 17 (AY17) and Rhodamine B (RhB) increased with increasing reaction temperature from 25 to 35 °C for all three $Na_{0.5}Bi_{0.5}FeO_3$ samples. For AY17, the degradation efficiency increased from 61.0%, 67.4%, and 74.6% at 25 °C to 69.2%, 77.1%, and 82.3% at 35 °C for the catalysts.

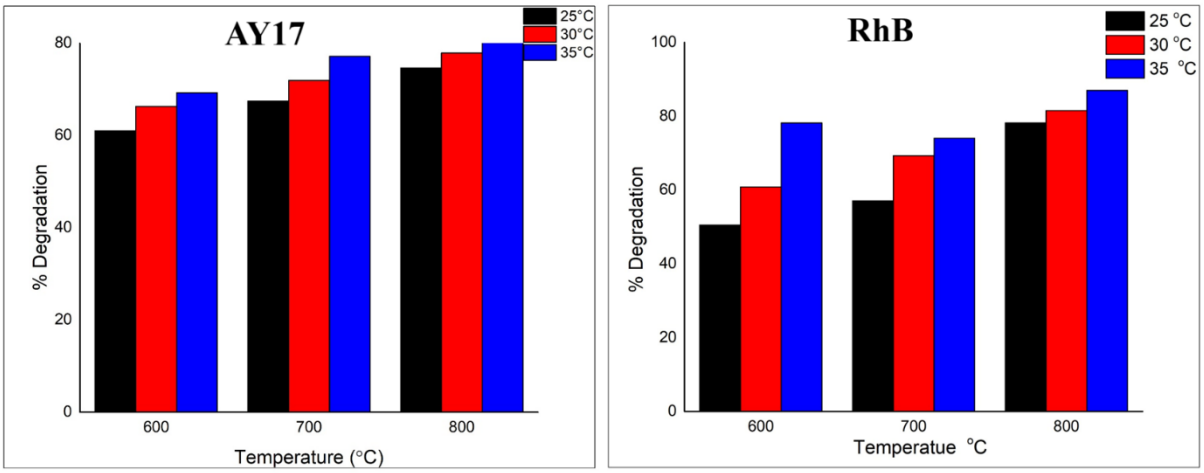


**Figure 11: Effect of temperature on the photocatalytic degradation of AY17 and RhB using $Na_{0.5}Bi_{0.5}FeO_3$ nanoparticles calcined at 600 °C. (Experimental conditions: [dye] = 40 ppm; catalyst dose = 0.75 g $L^{-1}$; temperature = 25, 30 and 35 °C; pH = 6.0 (AY 17) and 9.0 (RhB)]**

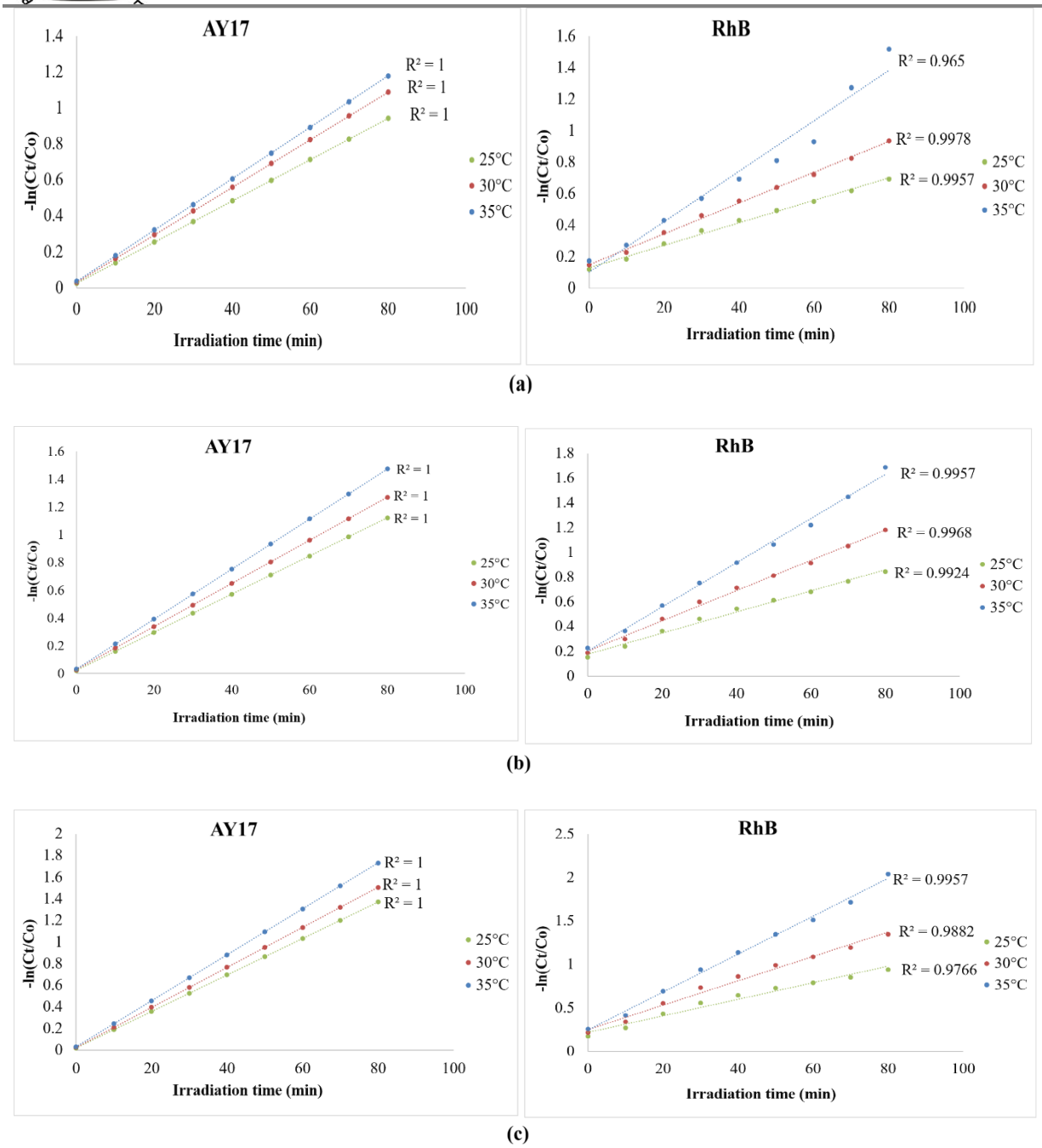


**Figure 12: Pseudo-first-order kinetic plots for the degradation of AY17 and RhB at different temperatures using $Na_{0.5}Bi_{0.5}FeO_3$ nanoparticles calcined at 600 °C. (Experimental conditions: [dye] = 40 ppm; catalyst dose = 0.75 g $L^{-1}$; temperature = 25, 30 and 35 °C; pH = 6.0 (AY 17) and 9.0 (RhB)]**

The corresponding apparent rate constants (Kapp) increased from 0.0115, 0.0138, and 0.0169 $min^{-1}$ to 0.0143, 0.0180, and 0.0213 $min^{-1}$. A similar trend was observed for RhB, with degradation increasing from 50.05%, 57.05%, and 61.0% at 25 °C to 78.13%, 81.50%, and 87.0% at 35 °C for the respective catalysts. These findings indicate that increasing reaction temperature enhanced the degradation of both dyes, potentially by accelerating reaction kinetics and improving interactions between dye molecules and the photocatalyst surface. For AY17, the enhanced degradation may also be associated with the increased generation or availability of ROS, particularly hydroxyl radicals, as reported previously [40–42]. Temperature-dependent behaviour has also been observed in ferrite-based dye-removal systems, where temperature influences dye–surface interactions and removal efficiency [39]. Comparatively, RhB showed a greater increase in degradation efficiency with rising temperature than AY17, particularly for the catalyst calcined at 600 °C. For both dyes, the 800 °C sample exhibited the highest degradation efficiency at each reaction temperature. This consistent trend suggests that calcination temperature plays an important role in photocatalytic performance, potentially through changes in the structural, optical, and charge-transfer properties of the catalyst, as reported for ferrite-

based photocatalysts [31–35,43]. Thus, 35 °C was the most effective reaction temperature among those investigated, and the 800 °C sample demonstrated the highest photocatalytic activity for both AY17 and RhB.

**Table 5: Comparison of Kobs for the degradation of AY17 and RhB at different reaction temperatures using $Na_{0.5}Bi_{0.5}FeO_3$ nanoparticles calcined at different temperatures. (Experimental conditions: [dye] = 40 ppm; catalyst dose = 0.75 g $L^{-1}$; temperature = 25, 30 and 35 °C; pH = 6.0 (AY 17) and 9.0 (RhB))]**

| Dye | Temperature (°C) | Reaction Temperature (°C) | $K_{obs}$ ($min^{-1}$) |
|---|---|---|---|
| AY17 | 600 | 25 | 0.0115 |
| | | 30 | 0.0132 |
| | | 35 | 0.0143 |
| | 700 | 25 | 0.0138 |
| | | 30 | 0.0156 |
| | | 35 | 0.018 |
| | 800 | 25 | 0.0169 |
| | | 30 | 0.0185 |
| | | 35 | 0.0213 |
| RhB | 600 | 25 | 0.0071 |
| | | 30 | 0.0098 |
| | | 35 | 0.016 |
| | 700 | 25 | 0.0086 |
| | | 30 | 0.0122 |
| | | 35 | 0.0178 |
| | 800 | 25 | 0.0095 |
| | | 30 | 0.014 |
| | | 35 | 0.0218 |

**Advanced Mechanistic Studies**

**Reactive Oxygen Species (ROS) Scavenging Study**

The degradation of Acid Yellow 17 (AY17) over $Na_{0.5}Bi_{0.5}FeO_3$ is proposed to begin with the adsorption of dye molecules onto the catalyst surface. Under visible-light exposure, the catalyst generates electron–hole pairs that initiate redox reactions. Electrons transferred to the conduction band react with dissolved oxygen, producing superoxide radicals ($\bullet O_2^-$). Meanwhile, valence-band holes can oxidize water molecules or hydroxide ions to form hydroxyl radicals (•OH). The superoxide radicals may further participate in the formation of $HO_2\bullet$ and $H_2O_2$, contributing to the generation of reactive oxidizing species. These reactive species attack the adsorbed dye molecules, resulting in their oxidative degradation through successive intermediate products and ultimately leading to mineralization into $CO_2$, $H_2O$ and inorganic ions [44-45].

$$AY17_{(aq)} + Na_{0.5}Bi_{0.5}FeO_3 \rightleftharpoons AY17_{(ads)} \quad \textbf{(2)}$$

$$Na_{0.5}Bi_{0.5}FeO_3 + h\nu \rightarrow e_{CB}^- + h_{VB}^+ \quad \textbf{(3)}$$

$$e_{CB}^- + O_2 \rightarrow \cdot O_2^- \quad \textbf{(4)}$$

$$h_{VB}^+ + H_2O \rightarrow \cdot OH + H^+ \quad \textbf{(5)}$$

$$h_{VB}^+ + OH^- \rightarrow \cdot OH \quad \textbf{(6)}$$

$$\cdot O_2^- + H^+ \rightarrow HO_2^{\cdot} \quad \textbf{(7)}$$

$$2HO_2^{\cdot} \rightarrow H_2O_2 + O_2 \quad \textbf{(8)}$$

$$AY17_{(ads)} + h^+ / \cdot OH / \cdot O_2^- \rightarrow \text{oxidized intermediates} \quad \textbf{(9)}$$

$$\text{oxidized intermediates} \rightarrow CO_2 + H_2O + \text{inorganic ions} \quad \textbf{(10)}$$

The proposed mechanism of Rhodamine B (RhB) photodegradation over $Na_{0.5}Bi_{0.5}FeO_3$ nanoparticles under visible-light irradiation is presented in Equations (11) to (17). During visible-light irradiation, $Na_{0.5}Bi_{0.5}FeO_3$ absorbs incident photons, causing electrons to move from the valence band to the conduction band and leaving holes in the valence band. The excited electrons interact with dissolved oxygen to generate superoxide radical anions ($\bullet O_2^-$), while the photogenerated holes react with water and hydroxide ions to produce hydroxyl radicals ($\bullet OH$). These reactive oxygen species, along with the electron-hole pairs, contribute

to the oxidative transformation of Rhodamine B (RhB) molecules. The degradation of adsorbed RhB can proceed through structural transformation involving N-deethylation and/or cleavage of the chromophoric structure, resulting in the formation of various oxidized and partially degraded intermediates. N-deethylation of RhB has been widely reported during photocatalytic transformation, while chromophore cleavage represents another important degradation pathway. The resulting intermediates can undergo further oxidation, aromatic-ring transformation and ring-opening reactions, producing progressively smaller organic molecules. Continued oxidation of these products can ultimately lead to mineralization, producing $CO_2$, $H_2O$ and inorganic products. Similar RhB degradation pathways involving deethylation, ring opening and subsequent mineralization have been reported using different photocatalytic systems.

$$Na_{0.5}Bi_{0.5}FeO_3 + h\nu \rightarrow e_{CB}^- + h_{VB}^+ \quad \textbf{(11)}$$

$$e_{CB}^- + O_2 \rightarrow \cdot O_2^- \quad \textbf{(12)}$$

$$h_{VB}^+ + H_2O \rightarrow \cdot OH + H^+ \quad \textbf{(13)}$$

$$h_{VB}^+ + OH^- \rightarrow \cdot OH \quad \textbf{(14)}$$

$$RhB_{(ads)} + h^+ / \bullet OH / \bullet O_2^- \rightarrow \text{oxidized intermediates, including N-deethylated and/or chromophore-cleaved intermediates} \quad \textbf{(15)}$$

$$\text{N-deethylated/chromophore-cleaved intermediates} \rightarrow \text{aromatic intermediates} \rightarrow \text{smaller organic products} \quad \textbf{(16)}$$

$$\text{Smaller organic products} \rightarrow CO_2 + H_2O + \text{inorganic product} \quad \textbf{(17)}$$

The proposed mechanism is also consistent with the photocatalytic behaviour reported in the earlier studies [46-53]. The higher photocatalytic performance of the samples calcined at higher temperature can be associated with their improved crystallinity, visible-light absorption and reduced optical band gap, which facilitate the generation and utilization of photogenerated charge carriers.

**Mineralization Analysis (TOC/COD)**

The extent of dye mineralization was assessed by determining the total organic carbon (TOC) content. In the case of Acid Yellow 17, photocatalytic treatment promotes the breakdown of the azo linkage (–N=N–) within the dye structure, generating intermediate compounds that undergo subsequent oxidation. Similarly, for RhB, the cleavage of the xanthene ring to form smaller organic fragments initiated by photocatalytic process. These reactions can progressively convert the organic intermediates into simpler end products, including carbon dioxide and water. TOC measurement is therefore an important indicator of mineralization, as it helps quantify the decrease in residual organic carbon during treatment. The analysis of TOC reduction following treatment

ISSN No. 2454-6194 | DOI: 10.51584/IJRIAS |Volume XI Issue XI November 2026

with the as-prepared $Na_{0.5}Bi_{0.5}FeO_3$ nanoparticles showed that mineralization efficiency increased with increasing calcination temperature. Specifically, the mineralization percentages achieved are 67%, 73.67%, and 79% for AY 17 and 71.20%, 80%, and 85.30% for RhB with the photocatalysts calcined at 600 °C, 700 °C, and 800 °C, respectively. This progressive trend indicates the greater reactivity and structural efficiency of the synthesized $Na_{0.5}Bi_{0.5}FeO_3$ photocatalyst when calcined at 800 °C.

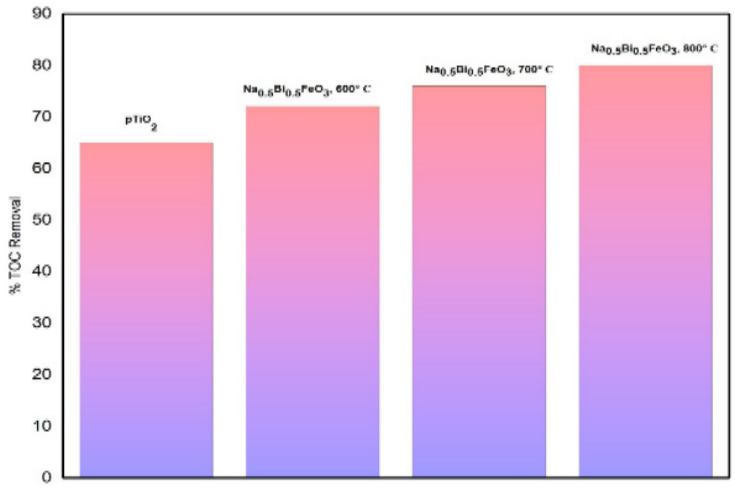


**(A)**

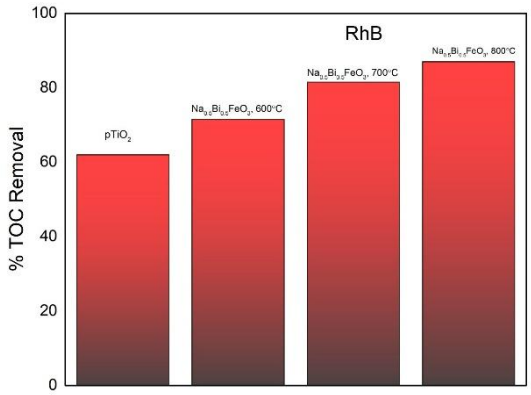


**(B)**

**Figure 13: TOC removal from AY17 dye solution during photocatalytic degradation using the prepared catalyst (A) AY 17 (B) RhB. (Experimental conditions: [dye] = 40mgL$^{-1}$, catalyst dose = 0.75gL$^{-1}$, pH=6.0 (AY 17) and 9.0 (RhB), Temperature = 308K).**

**Catalyst Reusability and Stability**

To assess the reusability of the prepared Na0.5Bi0.5FeO3 catalyst, we conducted five recycling runs. The recovered catalyst was cleansed with boiling water until the filtrate became clear.

Then, the filtrate catalyst was dried in an air oven at 95°C to 100°C and then recalcined in a muffle furnace at 500 °C.

After 5 cycles, dye removal efficiency decreased from 79% to 68% for AY17 and 87% to to 69% for RhB (Fig. 14). This study suggests that the photocatalyst is highly stable during photocatalytic degradation, and the reason for the decline in the removal capacity of the catalyst is due to the deposition of photo-insensitive hydroxide ions on the surface, blocking its active sites.

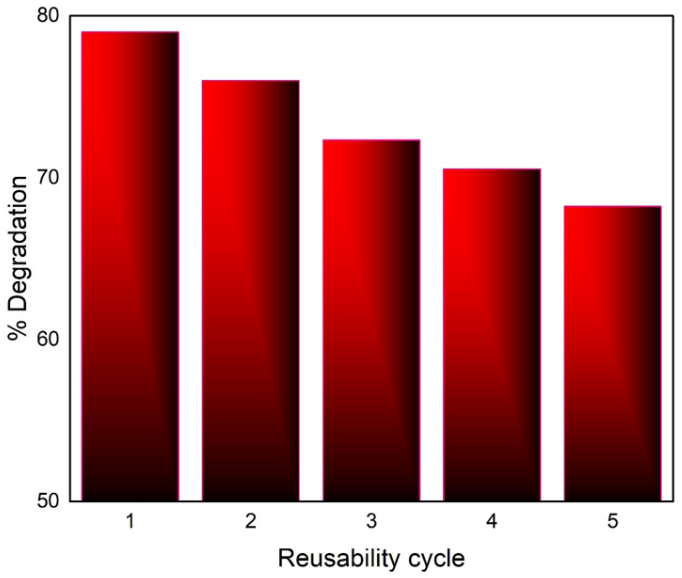


(A)

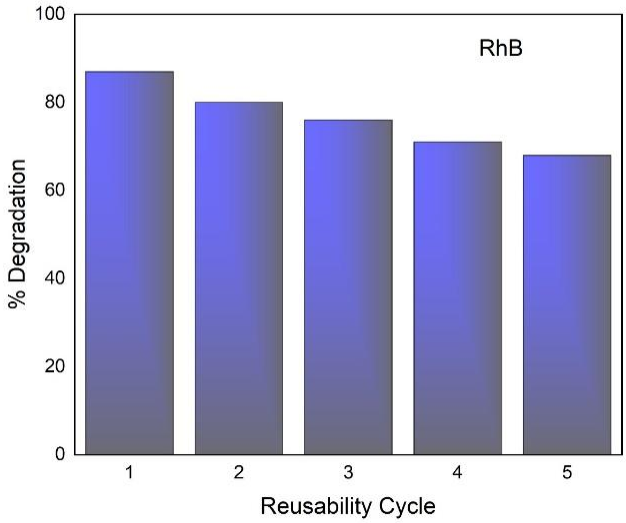


(B)

**Figure 14: Reusability and stability evaluation of the $Na_{0.5}Bi_{0.5}FeO_3$ catalyst, showing percentage degradation after each run (A) AY 17 and (B) RhB (cycles 1-5). (Experimental conditions: [dye] = 40mgL$^{-1}$, catalyst dose = 0.75gL$^{-1}$, pH=6.0 (AY 17) and 9.0 (RhB), Temperature = 308K).**

Hence, after a comprehensive evaluation of all operational parameters, it is evident that the $Na_{0.5}Bi_{0.5}FeO_3$ catalyst calcined at 800 °C exhibited the most outstanding photocatalytic performance. This superior performance is primarily attributed to its optimally narrow bandgap (1.85 eV) compared to the samples calcined at lower temperatures (2.04 eV for 700 °C and 2.10 eV for 600 °C), which significantly facilitates maximum visible-light absorption and efficient charge carrier generation. Furthermore, following its successful synthesis via the sol-gel method, the present study effectively establishes the practical viability of this highly active catalyst for environmental remediation and deep mineralization.

## CONCLUSION

The present study comparatively investigated the photocatalytic degradation of Acid Yellow 17 (AY17) and Rhodamine B (RhB) using $Na_{0.5}Bi_{0.5}FeO_3$ nanoparticles calcined at 600, 700, and 800 °C under visible-light

irradiation. The results demonstrated that photocatalytic activity improved with increasing calcination temperature, with the 800 °C sample exhibiting the highest degradation efficiency for both dyes. The degradation efficiencies reached a maximum of 79% for AY17 and 87% for RhB, indicating that RhB was more readily degraded under the investigated conditions. Both dyes showed maximum degradation at an initial concentration of 40 mg $L^{-1}$ and a catalyst dose of 0.75 g $L^{-1}$. Increase in the dye concentration or the catalyst dose resulted in reduced degradation efficiency, possibly because of decreased light penetration, increased light scattering, and catalyst particle agglomeration. The optimum pH differed between the dyes, with pH 6 favouring AY17 degradation and pH 9 favouring RhB degradation. This difference may be associated with the ionic characteristics of the dyes and their electrostatic interactions with the catalyst surface. Furthermore, increasing the reaction temperature from 25 to 35 °C enhanced the degradation of both dyes, with the highest efficiencies observed at 35 °C. The kinetic results showed good agreement with the pseudo-first-order model.

The proposed photocatalytic process involves the formation of electron–hole pairs upon exposure to visible light, followed by the formation of reactive oxygen species that participate in dye oxidation. Hydroxyl radicals, superoxide radical anions and photogenerated holes are proposed to contribute to the degradation of both dyes through successive oxidation and transformation of intermediate products. The observed temperature-dependent enhancement in photocatalytic activity also indicates that reaction conditions influence the overall degradation process. Therefore, $Na_{0.5}Bi_{0.5}FeO_3$ nanoparticles, particularly the sample calcined at 800 °C, demonstrated promising photocatalytic performance for the removal of both anionic and cationic dyes. The findings highlight the importance of optimising reaction parameters for effective dye degradation and support further investigation of this material for wastewater treatment applications.

## REFERENCES

1. Moses, J.; Ammayappan, L. Growth of Textile Industry and Their Issues on Environment with Reference to Wool Industry. *Res.* **2006**, *3*, 61–67.
2. Yaseen, D. A.; Scholz, M. Textile Dye Wastewater Characteristics and Constituents of Synthetic Effluents: A Critical Review. *Int. J. Environ. Sci. Technol.* **2019**, *16*, 1193–1226. https://doi.org/10.1007/s13762-018-2130-z.
3. Das, S.; Cherwoo, L.; Singh, R. Decoding Dye Degradation: Microbial Remediation of Textile Industry Effluents. *Biotechnol. Notes* **2023**, *4*, 64–76. https://doi.org/10.1016/j.biotno.2023.10.001.
4. Drumond Chequer, F. M.; de Oliveira, G. A. R.; Anastacio Ferraz, E. R.; Carvalho, J.; Boldrin Zanoni, M. V.; de Oliveir, D. P. Textile Dyes: Dyeing Process and Environmental Impact. In *Eco-Friendly Textile Dyeing and Finishing*; InTech, 2013; pp 151–176. https://doi.org/10.5772/53659.
5. Ranjithkumar, V.; Hazeen, A. N.; Thamilselvan, M.; Vairam, S. Magnetic Activated Carbon-Fe3O4 Nanocomposites—Synthesis and Applications in the Removal of Acid Yellow Dye 17 from Water. *Journal of Nanoscience and Nanotechnology* **2014**, *14* (7), 4949–4959. https://doi.org/10.1166/jnn.2014.9068.
6. Lackey, L.; Minesjr, R.; Mccreanor, P. Ozonation of acid yellow 17 dye in a semi-batch bubble column. *Journal of Hazardous Materials* **2006**, *138* (2), 357–362. https://doi.org/10.1016/j.jhazmat.2006.05.116.
7. Huda, A.; Suman, P. H.; Torquato, L. D. M.; Silva, B. F.; Handoko, C. T.; Gulo, F.; Zanoni, M. V. B.; Orlandi, M. O. Visible light-driven photoelectrocatalytic degradation of acid yellow 17 using Sn3O4 flower-like thin films supported on Ti substrate (Sn3O4/TiO2/Ti). *Journal of Photochemistry and Photobiology a Chemistry* **2019**, *376*, 196–205. https://doi.org/10.1016/j.jphotochem.2019.01.039.
8. Teli, M. D.; Nadathur, G. T. Adsorptive removal of acid yellow 17 (an anionic dye) from water by novel ionene chloride modified electrospun silica nanofibres. *Journal of Environmental Chemical Engineering* **2018**, *6* (6), 7257–7272. https://doi.org/10.1016/j.jece.2018.10.005.
9. Isik, B. Adsorptive removal of hazardous rhodamine B dye from aqueous solutions by St. John's wort (Hypericum perforatum). *Biomass Conversion and Biorefinery* **2024**, *15* (6), 9553–9564. https://doi.org/10.1007/s13399-024-05840-7.
10. Al-Gheethi, A. A.; Azhar, Q. M.; Kumar, P. S.; Yusuf, A. A.; Al-Buriahi, A. K.; Mohamed, R. M. S. R.; Al-Shaibani, M. M. Sustainable approaches for removing Rhodamine B dye using agricultural waste adsorbents: A review. *Chemosphere* **2021**, *287* (Pt 2), 132080. https://doi.org/10.1016/j.chemosphere.2021.132080.

11. Imam, S. S.; Babamale, H. F. A short review on the removal of rhodamine B dye using agricultural Waste-Based adsorbents. *Asian Journal of Chemical Sciences* **2020**, 25–37. https://doi.org/10.9734/ajocs/2020/v7i119013.
12. Jinendra, U.; Bilehal, D.; Nagabhushana, B. M.; Kumar, A. P. Adsorptive removal of Rhodamine B dye from aqueous solution by using graphene–based nickel nanocomposite. *Heliyon* **2021**, *7* (4), e06851. https://doi.org/10.1016/j.heliyon.2021.e06851.
13. Farhan, A. M.; Zaghair, A. M.; Abdullah, H. I. Adsorption study of rhodamine –B dye on plant (Citrus leaves). *Baghdad Science Journal* **2022**, *19* (4), 0838. https://doi.org/10.21123/bsj.2022.19.4.0838.
14. Waghchaure, R. H.; Adole, V. A.; Jagdale, B. S. Photocatalytic degradation of methylene blue, rhodamine B, methyl orange and Eriochrome black T dyes by modified ZnO nanocatalysts: A concise review. *Inorganic Chemistry Communications* **2022**, *143*, 109764. https://doi.org/10.1016/j.inoche.2022.109764.
15. Jamel, H. O.; Jasim, M. H.; Mahdi, M. A.; Ganduh, S. H.; Batool, M.; Jasim, L. S.; Haider, M. N. Adsorption of Rhodamine B dye from solution using 3-((1-(4-((1H-benzo[d]imidazol-2-yl)amino)phenyl)ethylidene)amino)phenol (BIAPEHB)/ P(AA-co-AM) composite. *Desalination and Water Treatment* **2025**, *321*, 101019. https://doi.org/10.1016/j.dwt.2025.101019.
16. Kurniawan, I.; Rahman, D. Y.; Hanafi, F.; Rahman, M. I.; Suryana, A. T.; Lestari, A.; Alifia, K. A.; Ichwani, R.; Turmuzi, M.; Huda, A. High stability and performance of organic pollutant removal using PVDF-TiO2 fabricated by non-solvent Induced phase separation process. *Journal of Ecological Engineering* **2026**, *27* (5), 430–443. https://doi.org/10.12911/22998993/216130.
17. Kamenická, B.; Švec, P.; Weidlich, T. Separation of Anionic Chlorinated Dyes from Polluted Aqueous Streams Using Ionic Liquids and Their Subsequent Recycling. *International Journal of Molecular Sciences* **2023**, *24* (15), 12235. https://doi.org/10.3390/ijms241512235.
18. De Oliveira Lopes, D.; Santos, L. O.; Nascimento, E. D.; De Souza, A. D. V.; De Oliveira Carvalho, F. A. Adsorption of acid yellow dye 17 on activated carbon prepared from Euterpe oleracea: kinetic and thermodynamic studies. *Research Society and Development* **2022**, *11* (2), e16511225556. https://doi.org/10.33448/rsd-v11i2.25556.
19. Lesniewicz, A.; Lewandowska-Andralojc, A. Probing mechanism of Rhodamine B decolorization under homogeneous conditions via pH-controlled photocatalysis with anionic porphyrin. *Scientific Reports* **2024**, *14* (1), 22600. https://doi.org/10.1038/s41598-024-73586-3.
20. Sivaguru, P.; Balakumar, S. The Adsorption of Rhodamine B Dye from Aqueous Solutions via Statistical Optimization. Rasayan J. Chem. 2024, 17, 905–915. https://doi.org/10.31788/RJC.2024.1738870.
21. Kalikeri, S.; Kodialbail, V. S. Auto-combustion synthesis of narrow band-gap bismuth ferrite nanoparticles for solar photocatalysis to remediate azo dye containing water. *Environmental Science and Pollution Research* **2020**, *28* (10), 12144–12152. https://doi.org/10.1007/s11356-020-10879-w.
22. Ghahfarokhi, S. E. M.; Helfi, K.; Shoushtari, M. Z. Synthesis of the Single-Phase bismuth ferrite (BIFEO3) nanoparticle and investigation of their structural, magnetic, optical and photocatalytic properties. *www.ajchem-a.com* **2022**. https://doi.org/10.22034/ajca.2021.309069.1284.
23. Ponraj, C.; Vinitha, G.; Daniel, J. Photocatalytic degradation of acid red-85 dye by nickel substituted bismuth ferrite nanoparticles. *Materials Research Express* **2019**, *6* (8), 084006. https://doi.org/10.1088/2053-1591/ab225f.
24. Farooq, M.; Ramli, A.; Naeem, A.; Shah, L. A.; Mahmood, T.; Tariq, M.; Khan, J.; Perveen, F.; Humayun, M. Photo-catalytic degradation of Acid Yellow 17 azo dye using ZrO2-CeO2 hollow microspheres as a catalyst. *Desalination and Water Treatment* **2019**, *170*, 318–324. https://doi.org/10.5004/dwt.2019.24685.
25. Huda, A.; Suman, P. H.; Torquato, L. D. M.; Silva, B. F.; Handoko, C. T.; Gulo, F.; Zanoni, M. V. B.; Orlandi, M. O. Visible light-driven photoelectrocatalytic degradation of acid yellow 17 using Sn3O4 flower-like thin films supported on Ti substrate (Sn3O4/TiO2/Ti). *Journal of Photochemistry and Photobiology a Chemistry* **2019**, *376*, 196–205. https://doi.org/10.1016/j.jphotochem.2019.01.039.
26. Kalikeri, S.; Kodialbail, V. S. Solar light-driven photocatalysis using mixed-phase bismuth ferrite (BiFeO3/Bi25FeO40) nanoparticles for remediation of dye-contaminated water: kinetics and comparison with artificial UV and visible light-mediated photocatalysis. *Environmental Science and Pollution Research* **2018**, *25* (14), 13881–13893. https://doi.org/10.1007/s11356-018-1291-0.

27. Khanna, A.; K, V. S. Solar photocatalysis for treatment of Acid Yellow-17 (AY-17) dye contaminated water using Ag@TiO2 core–shell structured nanoparticles. *Environmental Science and Pollution Research* **2013**, *20* (8), 5692–5707. https://doi.org/10.1007/s11356-013-1582-4.
28. Irfan, S.; Zhuanghao, Z.; Li, F.; Chen, Y.-X.; Liang, G.-X.; Luo, J.-T.; Ping, F. Critical review: Bismuth ferrite as an emerging visible light active nanostructured photocatalyst. *Journal of Materials Research and Technology* **2019**, *8* (6), 6375–6389. https://doi.org/10.1016/j.jmrt.2019.10.004.
29. Siddique, M.; Khan, N. M.; Saeed, M. Photocatalytic activity of bismuth ferrite nanoparticles synthesized via Sol-Gel route. *Zeitschrift Für Physikalische Chemie* **2018**, *233* (5), 595–607. https://doi.org/10.1515/zpch-2018-1225.
30. Soltani, T.; Entezari, M. H. Sono-synthesis of bismuth ferrite nanoparticles with high photocatalytic activity in degradation of Rhodamine B under solar light irradiation. *Chemical Engineering Journal* **2013**, *223*, 145–154. https://doi.org/10.1016/j.cej.2013.02.124.
31. Karnaji; Nurhasanah, I. Photodegradation of Rhodamine B by using ZnFe2O4 Nanoparticles Synthesized through Precipitation Method. *IOP Conference Series Materials Science and Engineering* **2017**, *202*, 012044. https://doi.org/10.1088/1757-899x/202/1/012044
32. Saidani, Amira, et al. "Effect of calcination temperature on the photocatalytic activity of precipitated ZnO nanoparticles for the degradation of rhodamine B under different light sources." *Water* 17.1 (2024): 32.
33. Dhiwahar, A. T.; Maruthamuthu, S.; Marnadu, R.; Sundararajan, M.; Manthrammel, M. A.; Shkir, M.; Sakthivel, P.; Reddy, V. R. M. Improved photocatalytic degradation of rhodamine B under visible light and magnetic properties using microwave combustion grown Ni doped copper ferrite spinel nanoparticles. *Solid State Sciences* **2021**, *113*, 106542. https://doi.org/10.1016/j.solidstatesciences.2021.106542.
34. Zhao, Y.; Xu, M.; Ji, Y.; Dong, Y.; Xing, G.; Xia, P.; Li, X.; He, W.; Qiao, L. Enhanced photocatalytic activities for degradation of dyes and drugs by crystalline bismuth Ferrite-Modified Graphene Hybrid Aerogel. *Crystals* **2022**, *12* (11), 1604. https://doi.org/10.3390/cryst12111604.
35. Wang, Mingjun, et al. "Influence of calcination temperature on photocatalyst performances of floral Bi2O3/TiO2 composite." *Catalysts* 12.12 (2022): 1635.
36. Nair, V. R.; Kodialbail, V. S. Floating bed reactor for visible light induced photocatalytic degradation of Acid Yellow 17 using polyaniline-TiO2 nanocomposites immobilized on polystyrene cubes. *Environmental Science and Pollution Research* **2020**, *27* (13), 14441–14453. https://doi.org/10.1007/s11356-020-07959-2.
37. Tariq, M.; Khan, J. Inquest of efficient photo-assist advanced oxidation processes (AOPs) for removal of azo dye (acid yellow 17) in aqueous medium: a comprehensive study on oxidative decomposition of AY 17. *SN Applied Sciences* **2020**, *2* (11). https://doi.org/10.1007/s42452-020-03701-2.
38. Flores, A.; Nesprias, K.; Vitale, P.; Tasca, J.; Lavat, A.; Eyler, N.; Cañizo, A. Heterogeneous Photocatalytic Discoloration/Degradation of Rhodamine B with H2O2 and Spinel Copper Ferrite Magnetic Nanoparticles. *Australian Journal of Chemistry* **2013**, *67* (4), 609–614. https://doi.org/10.1071/ch13435.
39. Al-Wasidi, A. S.; AlReshaidan, S. Enhanced Removal of Rhodamine b Dye from Aqueous Media via Adsorption on Facilely Synthesized Zinc Ferrite Nanoparticles. *Inorganics* **2024**, *12* (7), 191. https://doi.org/10.3390/inorganics12070191.
40. Khan, J.; Sayed, M.; Ali, F.; Khan, H. M. Removal of acid yellow 17 dye by fenton oxidation process. *Zeitschrift Für Physikalische Chemie* **2018**, *232* (4), 507–525. https://doi.org/10.1515/zpch-2017-1072.
41. Khan, J.; Tariq, M.; Muhammad, M.; Mehmood, M. H.; Ullah, I.; Raziq, A.; Akbar, F.; Saqib, M.; Rahim, A.; Niaz, A. Kinetic and thermodynamic study of oxidative degradation of acid yellow 17 dye by Fenton-like process: Effect of HCO3−, CO32−, Cl− and SO42− on dye degradation. *Bulletin of the Chemical Society of Ethiopia* **2019**, *33* (2), 243. https://doi.org/10.4314/bcse.v33i2.5.
42. Tariq, M.; Khan, J. Inquest of efficient photo-assist advanced oxidation processes (AOPs) for removal of azo dye (acid yellow 17) in aqueous medium: a comprehensive study on oxidative decomposition of AY 17. *SN Applied Sciences* **2020**, *2* (11). https://doi.org/10.1007/s42452-020-03701-2.
43. Miao, Z.; Tian, Y.; Li, S.; Ding, Z.; Chen, X.; Ma, W.; Chang, Y. Photocatalytic degradation of Rhodamine B over popcorn-like ZnFe2O4/CdS–GO ternary composite. *Journal of Materials Research and Technology* **2022**, *21*, 1863–1877. https://doi.org/10.1016/j.jmrt.2022.10.035.

44. Mehta, V. K. M. V. K. Photocatalytic Degradation of Commercially Important Dye Acid yellow 36 byCeFeO3. *International Journal of Engineering and Science Invention* **2025**, *14* (5), 9–14. https://doi.org/10.35629/6734-14050914.
45. Tariq, M.; Khan, J. Inquest of efficient photo-assist advanced oxidation processes (AOPs) for removal of azo dye (acid yellow 17) in aqueous medium: a comprehensive study on oxidative decomposition of AY 17. *SN Applied Sciences* **2020**, *2* (11). https://doi.org/10.1007/s42452-020-03701-2.
46. Nguyen, H. T.; Doan, V.-D.; Nguyen, T. L. H.; Nguyen, A.-T.; Tran, Q.-H.; Tran, V. A.; Le, V. T. Mechanistic pathway and optimization of rhodamine B degradation using Mn 3 O 4 /ZnO nanocomposite on microalgae-based carbon. *RSC Advances* **2025**, *15* (8), 6241–6259. https://doi.org/10.1039/d5ra00625b.
47. Wei, Z.; Lin, W.; Ding, Z.; Hou, B.; Wang, Y.; Wu, Y.; Chai, X. Photothermal-Assisted Photocatalytic degradation of rhodamine B using FE 3 O 4 /ZNIN 2 S 4 Type-II Heterojunction: Mechanism and Performance. *Langmuir* **2026**, *42* (5), 3923–3936. https://doi.org/10.1021/acs.langmuir.5c05233.
48. Abouri, M.; Benzaouak, A.; Elouardi, M.; Hamdaoui, L. E.; Zaaboul, F.; Azzaoui, K.; Hammouti, B.; Sabbahi, R.; Jodeh, S.; Belghiti, M. A. E.; Hamidi, A. E. Enhanced photocatalytic degradation of Rhodamine B using polyaniline-coated XTiO3(X = Co, Ni) nanocomposites. *Scientific Reports* **2025**, *15* (1), 3595. https://doi.org/10.1038/s41598-024-83610-1.
49. Jhansi, K.; Pujitha, M.; Venkateswarlu, B.; Swaminathan, P. Evaluation of photocatalytic degradation of rhodamine B using manganese zinc ferrite catalyst. *Next Research.* **2025**, *2* (3), 100686. https://doi.org/10.1016/j.nexres.2025.100686.
50. Chen, X.; Chen, X.; Li, B.; Ma, J.; Zhao, B.; Shao, N.; Wang, Y. Visible-light-induced degradation of rhodamine B by double Z-scheme magnetic ATP-g-C3N4/SnFe2O4/Bi2WO6 heterojunctions: Performance and mechanism. *Surfaces and Interfaces* **2024**, *49*, 104368. https://doi.org/10.1016/j.surfin.2024.104368.
51. Dhiwahar, A. T.; Maruthamuthu, S.; Marnadu, R.; Sundararajan, M.; Manthrammel, M. A.; Shkir, M.; Sakthivel, P.; Reddy, V. R. M. Improved photocatalytic degradation of rhodamine B under visible light and magnetic properties using microwave combustion grown Ni doped copper ferrite spinel nanoparticles. *Solid State Sciences* **2021**, *113*, 106542. https://doi.org/10.1016/j.solidstatesciences.2021.106542.
52. Som, I.; Roy, M.; Saha, R. Advances in nanomaterial-based water treatment approaches for photocatalytic degradation of water pollutants. *ChemCatChem* **2020**, *12* (13), 3409–3433. https://doi.org/10.1002/cctc.201902081.
53. Al-Hazemi, M. E.; Kashmiry, A. A. Synthesis of pure and highly doped (II-VI) semiconductor nanoparticles of Nickel for effective environmental remediation of Rhodamine-B dye from wastewater streams. *Journal of Dispersion Science and Technology* **2023**, *46* (3), 396–405. https://doi.org/10.1080/01932691.2023.2289624.